A Modulation Reference Compensation Method to Realize Fully Decoupled Power Control for Modular Multilevel Converters

Jinyu Wang, *Member, IEEE*, Peng Wang, *Fellow, IEEE*, Michael Zagrodnik, Suvajit Mukherjee, *Senior Member, IEEE*, and Dhanashree Vaidya

***Abstract*—This paper proposes a modulation reference compensation method to completely eliminate the intercoupling between the output active and reactive powers of modular multilevel converters (MMCs). Different from the existing methods, it is realized not based on an accurate control model, but by directly amending the initial arm modulation references of MMCs. Therefore, the proposed method is essentially a compensation algorithm, which is extremely easy to implement in a microcontroller with low calculation burden. In addition, it does not need any additional closed-loop controllers or voltage/current sensors, which is very beneficial to practical projects. The proposed method finally realizes accurate and fully decoupled active and reactive power regulation, avoids overload operation and protection malfunction, and significantly improves the dynamic performance of MMCs. The effectiveness and accuracy of the proposed analysis and compensation method are carefully verified by both simulation and experimental results.**

***Index Terms*—Compensation method, high-voltage direct-current (HVdc) transmission, modular multilevel converter (MMC), parameter design, power decoupling.**

I. Introduction

A MODULAR multilevel converter (MMC) has gained immense popularity in not only high-voltage direct-current (HVdc) transmission [1], [2], but also variable-speed motor drives [3], static compensators (STATCOMs) [4], energy storage systems [5], and flexible ac transmission systems [6], owing to some distinctive advantages, e.g., modularity structure, flexible expandability, excellent output waveforms, low switching losses, and high reliability.

Manuscript received May 15, 2018; revised July 20, 2018 and October 1, 2018; accepted November 1, 2018. Date of publication November 7, 2018; date of current version May 22, 2019. This work was supported by the Rolls-Royce @NTU Corporate Lab, Nanyang Technological University, Singapore. Recommended for publication by Associate Editor M. A. Perez. *(Corresponding author: Jinyu Wang.)*

J. Wang and D. Vaidya are with the Rolls-Royce @NTU Corporate Lab, Nanyang Technological University, Singapore 639798 (e-mail:

decoupling capability is much better than the classical one, this method still cannot fully realize the power decoupling of MMCs because of the marginally stable property. Another power decoupling control method is realized by cutting off three new found coupling paths among electrical quantities inside MMCs [10]. These new coupling paths are identified by deriving an accurate ac current control model of MMCs in the *dq* rotating frame. Although this method can finally realize fully decoupled power control, it is rather complex, and its dynamic and stability are highly related to the phase-locked loop (PLL).

As introduced above, other than the classical one, the existing power decoupling control methods of MMCs are all based on the established accurate ac current control model in the rotating frame. The derivation is really tedious, and the calculation burden is really heavy considering the complex relationship of the electrical quantities and control strategies inside the MMCs.

This paper proposes a very simple method to realize the fully decoupled power control for MMCs. It is realized by forcing the inner electromotive force (EMF) of MMCs to be exactly equal to the given modulation reference, regardless of all the complex internal coupling effects. This method is neither depending on the MMC accurate control model nor realized in the *dq* rotating frame, but essentially a compensation algorithm realized by directly amending the arm initial modulation references. Therefore, it is extremely easy to implement in a microcontroller with low calculation burden and not affected by the dynamic characteristics of the PLL. Moreover, this method does not need any additional closed-loop controllers or voltage/current sensors, and thus, extra control parameter design and cost are not needed, which is of great significance to practical projects. Results from a realistically sized grid-connected simulation model and a downscaled experimental platform confirm the effectiveness and accuracy of the theoretical analysis and the proposed compensation algorithm.

II. Existing Power Decoupling Control Methods for MMCs

A. Modular Multilevel Converter

The operation principle of MMCs has been extensively explained in [21]–[24] and thus will not be repeated here. The topology of a three-phase MMC is shown in Fig. 1. It has three phase legs connected in parallel to a common dc bus. Each phase leg has two arms: the upper arm and the lower arm. Each arm consists of n same half-bridge submodules (SMs), connected in series with an arm inductor. The SM is composed of two insulated-gate bipolar transistors (IGBTs) paralleled with a capacitor. Normally, the SM can output the capacitor voltage when it is inserted or zero when it is bypassed.

Fig. 2(a) shows the single-phase equivalent circuit of the MMC ignoring the switching actions of IGBTs. L and R are the arm series inductor and the arm equivalent resistor, respectively. L_c and R_c are the connecting inductor and the equivalent resistor between the point of common coupling and the MMC. u_j (i_j) is the ac-side voltage (current) of phase j ($j = a, b, c$). u_{pj} (u_{nj}) and i_{pj} (i_{nj}) are, respectively, the upper (lower) arm voltage and current. $U_{\rm dc}$ is the dc-bus voltage and $i_{{\rm diff}j}$ is the inner

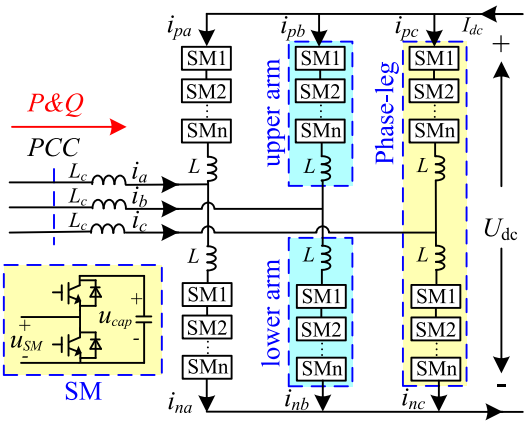

Fig. 1. Circuit topology of the MMC.

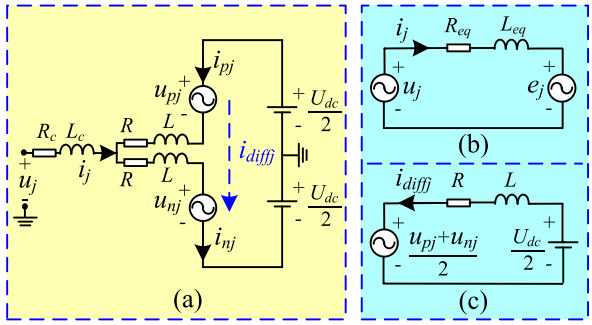

Fig. 2. Equivalent circuit of the MMC. (a) Single-phase equivalent circuit. (b) AC equivalent circuit. (c) DC equivalent circuit.

unbalanced current. e_j is the EMF of the MMC. According to the ac and dc equivalent circuits in Fig. 2(b) and (c), the MMC can be expressed as [18], [19]

$$u_j = e_j + R_{\rm eq} i_j + L_{\rm eq} \frac{di_j}{dt} \tag{1}$$

$$u_{{\rm diff}j} = R i_{{\rm diff}j} + L \frac{di_{{\rm diff}j}}{dt} = \frac{U_{\rm dc}}{2} - \frac{u_{pj} + u_{nj}}{2} \tag{2}$$

where e_j, $L_{\rm eq}$, and $R_{\rm eq}$ are $e_j = (u_{nj} - u_{pj})/2$, $L_{\rm eq} = L_c + L/2$, and $R_{\rm eq} = R_c + R/2$, respectively. $i_{{\rm diff}j} = (i_{pj} + i_{nj})/2 = I_{\rm dc}/3 + i_{{\rm cir}j}$, where $i_{{\rm cir}j}$ is the circulating current and $I_{\rm dc}$ is the dc-bus current. $u_{{\rm diff}j}$ is the difference voltage. To output the desired phase EMF $e_{j\_{\rm ref}}$, the reference voltages of the upper and lower arms of the MMC can be expressed as

$$\begin{cases} u_{jp\_{\rm ref}} = U_{\rm dc}/2 - e_{j\_{\rm ref}} - u_{{\rm cir}j\_{\rm ref}} \\ u_{jn\_{\rm ref}} = U_{\rm dc}/2 + e_{j\_{\rm ref}} - u_{{\rm cir}j\_{\rm ref}} \end{cases} \tag{3}$$

where $e_{j\_{\rm ref}}$ and $u_{cirj\_{\rm ref}}$ come from the ac current controller and the circulating current controller, respectively.

B. Existing Power Decoupling Control Methods for MMCs

This section briefly introduces the existing power decoupling control methods for MMCs, including the classical method [20], [26]–[28], and the two recently proposed methods mentioned in the introduction [9], [10].

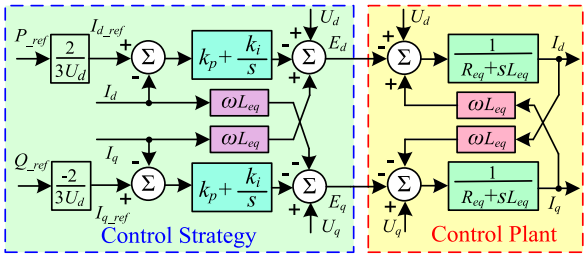

Fig. 3. Classical power decoupling control method for the MMC.

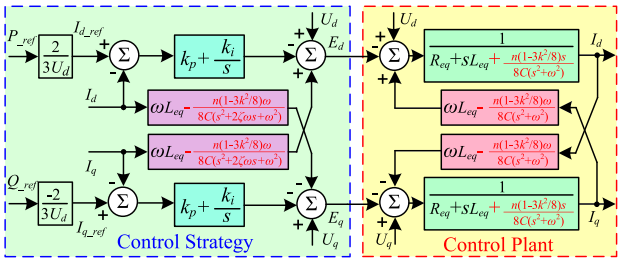

Fig. 4. Improved power decoupling control method for the MMC.

Fig. 3 presents the classical power decoupling control method for MMCs. The adopted control plant in Fig. 3 has the same form as the conventional VSCs, which has only one coupling path between the active and reactive powers. It is introduced by the frame transformation (from *abc* to *dq*) and can be completely eliminated by the cross-decoupling terms [7]. However, the adopted ac current control plant is derived without considering all the complex dynamics and interactions inside the MMC, which are significantly different from the conventional VSCs, and thus, the extra power coupling paths and the influence factors cannot be identified.

As shown in Fig. 4, an improved power decoupling control method for the MMC is proposed in [9]. This method is based on the newly established ac current control model considering the influence of the equivalent MMC ac capacitor. The n, k, C, and ω in the red terms are the total number of SMs per arm, modulation index, SM capacitor, and fundamental frequency of the MMC, respectively. The ζ is called damping index. When it equals zero, this method can realize full decoupling, while the system is marginally stable. When it is larger than zero, this method cannot realize full decoupling. Thus, the value of ζ should be chosen to achieve an acceptable system damping and decoupling performance. In addition, the modulation index k cannot be accurately determined, since it continuously changes with the operation conditions.

A full power decoupling control method for the MMC is proposed in [10]. Fig. 5 presents its newly established ac current control model. In Fig. 5, $Cou_{1d,q} = n(-U_{\rm dc}U_{c1d,q} \pm U_{c1d}U_{{\rm cir}q,d} - U_{c1q}U_{{\rm cird},q})/2$, $Cou_{3d,q} = nU_{c2d}/2$, and $Cou_{4d,q} = n(-U_{\rm dc}U_{c2d,q} \pm U_{c1d}E_{q,d} + U_{c1q}E_{d,q})/2$, where $U_{c1d,q}$, $U_{c2d,q}$, $U_{{\rm cird},q}$, and $E_{d,q}$ are the SM capacitor voltage first- and second-order components, and the outputs of the circulating current and ac current controllers in the *dq* rotating frame, respectively. This model is derived by transferring all

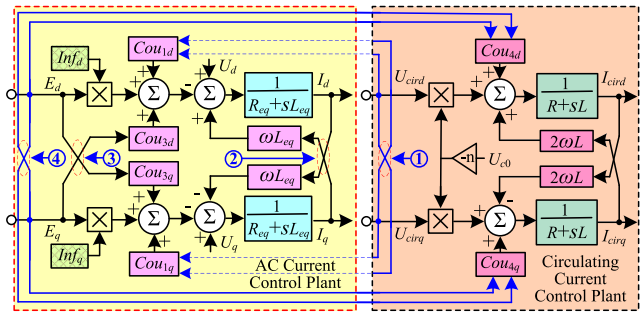

Fig. 5. Accurate current control model established in [10].

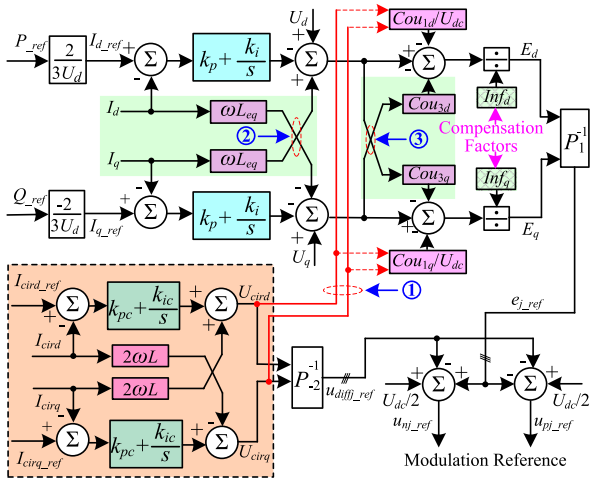

Fig. 6. Full power decoupling control method for the MMC.

the analytical expressions of the electrical quantities inside the MMC into the *dq* rotating frame, in which circulating current control is also considered. Therefore, it is a very accurate control model. Three new power coupling paths (①, ③, and ④) and two power influence factors ($\mathrm{Inf}_{d,q} = nU_{c0} \mp nU_{c2q}/2$) are identified. A corresponding decoupling strategy is proposed (in Fig. 6) to cut off the newly found coupling paths and offset the influence factors. This method is stable and can realize the fully decoupled power control. However, it is rather complex, and all the decoupling and compensations terms are obtained in the *dq* frame. Thus, multiple Park transformations have to be employed, and the dynamics are inevitably affected by the PLL.

III. Proposed Full Power Decoupling Control Method for MMCs

This section proposes a very simple compensation method to realize fully decoupled power control for MMCs. Before proposing the compensation method, the coupling effects among internal electrical quantities and control strategies of the MMC should be analyzed in detail. These derivations and analyzations are employed to reveal the essence of power coupling inside MMCs to explain the motivation/idea behind this compensation method, not to derive the accurate ac current control model.

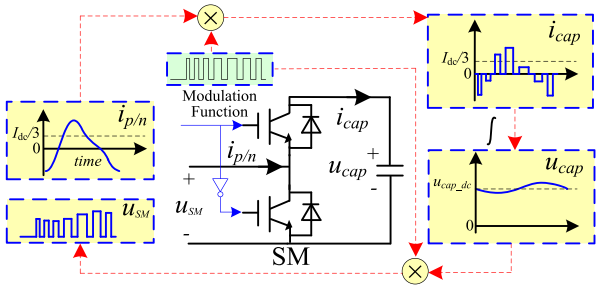

Fig. 7. Relationship of the electrical quantities in an SM.

A. Coupling Effects Among Internal Electrical Quantities and Control Strategies of the MMC

According to (3), the modulation functions of the upper and lower arms can be written as

$$\begin{cases} S_{pj} = [1 - M\sin(\omega t + \alpha_j)]/2 - M_{\rm cir}\sin(2\omega t + \beta_j) \\ S_{nj} = [1 + M\sin(\omega t + \alpha_j)]/2 - M_{\rm cir}\sin(2\omega t + \beta_j) \end{cases} \tag{4}$$

where $M = 2E/U_{\rm dc}$ and $M_{\rm cir} = 2U_{\rm cir}/U_{\rm dc}$. E and $U_{\rm cir}$ are the amplitudes of the EMF and the difference voltage of the MMC, respectively. α_j and β_j are the corresponding initial phase angles in phase *j*. In the analysis, only the dominated second circulating currents are considered, since the other higher order ones are negligibly small [19].

From Fig. 2(a), the currents of the upper and lower arms can be expressed as

$$\begin{cases} i_{pj} = I_{\rm dc}/3 - I\sin(\omega t + \varphi_j)/2 + I_{\rm cir}\sin(2\omega t + \theta_j) \\ i_{nj} = I_{\rm dc}/3 + I\sin(\omega t + \varphi_j)/2 + I_{\rm cir}\sin(2\omega t + \theta_j) \end{cases} \tag{5}$$

where I ($I_{\rm cir}$) and φ_j (θ_j) are the amplitude and initial phase angle of the ac current (circulating current) in phase *j*, respectively. Without loss of generality, although circulating current control strategy is employed, the circulating currents here are still considered because, to realize different control objectives, e.g., improve efficiency, limit peak arm currents, minimize capacitor voltage ripples, etc., circulating currents may not always be completely eliminated [18].

Fig. 7 presents the relationship among the electrical quantities in an SM through the modulation function. As shown in Fig. 7, the SM capacitor current, SM capacitor voltage, and the SM output voltage can be, respectively, expressed as

$$\begin{cases} i_{{\rm cap}\_pj} = S_{pj} i_{pj} \\ i_{{\rm cap}\_nj} = S_{nj} i_{nj} \end{cases} \tag{6}$$

$$\begin{cases} u_{{\rm cap}\_pj} = u_{c0} + \frac{1}{C}\int i_{{\rm cap}\_pj}\,dt \\ u_{{\rm cap}\_nj} = u_{c0} + \frac{1}{C}\int i_{{\rm cap}\_nj}\,dt \end{cases} \tag{7}$$

$$\begin{cases} u_{{\rm SM}\_pj} = S_{pj} u_{{\rm cap}\_pj} \\ u_{{\rm SM}\_nj} = S_{nj} u_{{\rm cap}\_nj} \end{cases} \tag{8}$$

where u_{c0} is the initial capacitor voltage. Since the *n* SMs per arm have approximately the same value after applying appropriate SM capacitor voltage-balancing strategy [30], [31], the upper and lower arm voltages can then be derived as

$$\begin{cases} u_{{\rm arm}\_pj} = n u_{{\rm SM}\_pj} \\ u_{{\rm arm}\_nj} = n u_{{\rm SM}\_nj}. \end{cases} \tag{9}$$

The phase EMF of the MMC equals the voltage difference between the lower arm and the upper arm. According to (4)–(9), e_j can be calculated as

$$e_j = (u_{{\rm arm}\_nj} - u_{{\rm arm}\_pj})/2 = e_{1j} + e_{3j} + e_{5j} \tag{10}$$

where e_{1j}, e_{3j}, and e_{5j} are the first-, third-, and fifth-order ac components of e_j, respectively, whose detailed analytical expressions can be derived as (11) shown at the bottom of this page, where $U_{\rm cap}$ is the dc component of the SM capacitor voltage, and its value is approximated to $U_{\rm dc}/n$. Although third- and fifth-order ac components exist in the EMF of MMCs, the third-order ac current component is generally excluded by a *Y*–Δ-connected transformer or eliminated by the control strategies [19], and the fifth-order ac current component is negligibly small [18]. Therefore, the transmitted active and reactive powers of MMCs can be seen as controlled by e_{1j}.

The first term at the right side of e_{1j} is the same as the conventional VSCs and equals the given modulation reference. The reason why the conventional VSCs have no additional power coupling is that its EMF only has this term. However, as to the MMC, other than the first term, there are other eight terms related to different internal electrical quantities and control strategies of the MMC because of the special topology and particular operation principle [10]. There are exactly the terms that introduce the complex coupling effects for the transmitted active and reactive powers.

$$\begin{cases} e_{1j} = \frac{1}{2}MnU_{\rm cap}\sin(\omega t + \alpha_j) - \frac{MnI_{\rm dc}}{12\omega C}\cos(\omega t + \alpha_j) + \frac{3MnI_{\rm cir}}{16\omega C}\sin(\omega t - \alpha_j + \theta_j) - \frac{nI}{8\omega C}\cos(\omega t + \varphi_j) \\ \quad + \frac{MM_{\rm cir}nI_{\rm dc}}{24\omega C}\sin(\omega t - \alpha_j + \beta_j) + \frac{M_{\rm cir}^2 nI}{12\omega C}\cos(\omega t + \varphi_j) - \frac{M^2 nI}{64\omega C}\cos(\omega t + \varphi_j) - \frac{MM_{\rm cir}nI_{\rm cir}}{8\omega C}\cos(\omega t + \alpha_j + \beta_j - \theta_j) \\ \quad + \frac{MM_{\rm cir}nI_{\rm cir}}{24\omega C}\cos(\omega t + \alpha_j + \theta_j - \beta_j) \\ e_{3j} = \frac{M^2 nI}{64\omega C}\cos(3\omega t + 2\alpha_j + \varphi_j) - \frac{5MnI_{\rm cir}}{48\omega C}\sin(3\omega t + \alpha_j + \theta_j) + \frac{M_{\rm cir}nI}{6\omega C}\sin(3\omega t + \beta_j + \varphi_j) \\ \quad + \frac{5MM_{\rm cir}nI_{\rm cir}}{32\omega C}\cos(3\omega t - \alpha_j + \beta_j + \theta_j) + \frac{3MM_{\rm cir}nI_{\rm dc}}{24\omega C}\sin(3\omega t + \alpha_j + \beta_j) - \frac{M_{\rm cir}^2 nI}{8\omega C}\cos(3\omega t + 2\beta_j - \varphi_j) \\ e_{5j} = -\frac{7MM_{\rm cir}nI_{\rm cir}}{96\omega C}\cos(5\omega t + \alpha_j + \beta_j + \theta_j) + \frac{M_{\rm cir}^2 nI}{24\omega C}\cos(5\omega t + 2\beta_j + \varphi_j) \end{cases} \tag{11}$$

B. Proposed Full Power Decoupling Control Method for MMCs

As analyzed in Section III-A, the essence of power coupling inside the MMC is that, different from the conventional VSCs, the EMF of MMCs does not exactly equal to the given modulation reference because of the coupling effects from the SM capacitor voltage, dc-bus current, circulating current, and the control strategies. Therefore, if it can be forced to be exactly equal to the given modulation reference, all the additional terms in e_{1j} of (11) can then be completely eliminated, so as their introduced coupling effects. This can be realized by simultaneously compensating or amending the initial modulation references of the upper and lower arms of the MMC. Assuming that $\Delta e_{j\_\mathrm{ref}}$ is the additional compensation factor, the modulation references of the upper and lower arms after being compensated can be expressed as

$$\begin{cases} u^c_{pj\_\mathrm{ref}} = U_{\mathrm{dc}}/2 - e_{j\_\mathrm{ref}} - \Delta e_{j\_\mathrm{ref}} - u_{\mathrm{cir}j\_\mathrm{ref}} \\ u^c_{nj\_\mathrm{ref}} = U_{\mathrm{dc}}/2 + e_{j\_\mathrm{ref}} + \Delta e_{j\_\mathrm{ref}} - u_{\mathrm{cir}j\_\mathrm{ref}} \end{cases} \tag{12}$$

where e_{j_ref} is the initial modulation reference of the MMC in phase j. It can be seen from (12) that the sign of the compensation factor $\Delta e_{j\_\mathrm{ref}}$ for the upper and lower arm modulation references is opposite. Only in this way, the added compensation factor can finally affect the EMF of MMCs (use their difference to control the ac current). The sign of the circulating current control factor $u_{\mathrm{cir}j\_\mathrm{ref}}$ for the upper and lower arm modulation references is the same. Only in this way, the circulating current control factor can finally control the circulating current (use their sum to control the circulating current). Therefore, the circulating current control (proportional–resonant controllers @ 2ω is employed in this paper) and the compensation algorithm are independent of each other.

The modulation functions of the upper and lower arms after being compensated are their normalized modulation references with a similar form as (4), which can be expressed as

$$\begin{cases} S^c_{pj\_\mathrm{ref}} = \frac{1}{2} - \frac{e_{j\_\mathrm{ref}}}{U_{\mathrm{dc}}} - \frac{\Delta e_{j\_\mathrm{ref}}}{U_{\mathrm{dc}}} - \frac{u_{\mathrm{cir}j\_\mathrm{ref}}}{U_{\mathrm{dc}}} \\ S^c_{nj\_\mathrm{ref}} = \frac{1}{2} + \frac{e_{j\_\mathrm{ref}}}{U_{\mathrm{dc}}} + \frac{\Delta e_{j\_\mathrm{ref}}}{U_{\mathrm{dc}}} - \frac{u_{\mathrm{cir}j\_\mathrm{ref}}}{U_{\mathrm{dc}}}. \end{cases} \tag{13}$$

The EMF of the MMC after being compensated can be derived as

$$e^c_j = (u^c_{\mathrm{arm}\_nj} - u^c_{\mathrm{arm}\_pj})/2 = (S^c_{nj\_\mathrm{ref}} u^{\Sigma}_{nj} - S^c_{pj\_\mathrm{ref}} u^{\Sigma}_{pj})/2 \tag{14}$$

where $u^{\Sigma}_{pj} = \sum_{i=1}^{n} u_{\mathrm{cap}\_pji}$ and $u^{\Sigma}_{nj} = \sum_{i=1}^{n} u_{\mathrm{cap}\_nji}$ are the total SM capacitor voltages of the upper and lower arms, respectively. To force the final EMF of MMCs to be exactly equal to the given initial modulation reference, the following equation should be fulfilled:

$$e^c_j = (S^c_{nj\_\mathrm{ref}} u^{\Sigma}_{nj} - S^c_{pj\_\mathrm{ref}} u^{\Sigma}_{pj})/2 = e_{j\_\mathrm{ref}}. \tag{15}$$

Thus, inserting (13) and (14) into (15), the compensation factor can be derived as

$$\Delta e_{j\_\mathrm{ref}} = \frac{2e_{j\_\mathrm{ref}} - (u^{\Sigma}_{nj} - u^{\Sigma}_{pj})/2}{(u^{\Sigma}_{nj} + u^{\Sigma}_{pj})/U_{\mathrm{dc}}} - e_{j\_\mathrm{ref}}. \tag{16}$$

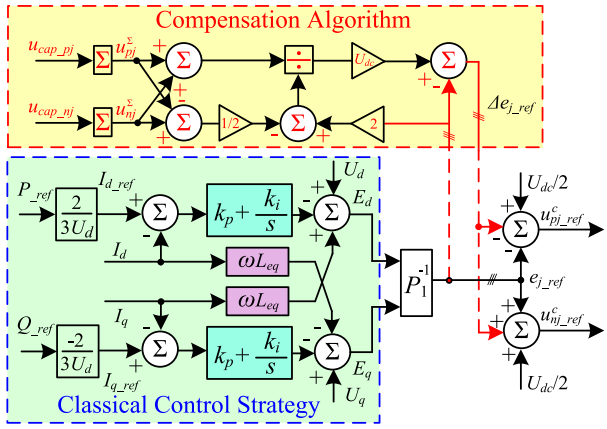

Fig. 8. Proposed full power decoupling control method for MMCs.

The compensation algorithm is depicted in Fig. 8. From Fig. 8, the proposed compensation algorithm is superposed on the classical power control method to finally realize the full power decoupling. Its structure is very simple, and the calculation burden is very low and thus is easy to implement in a microcontroller. Since the input variables are the SM capacitor voltages and the initial modulation reference, extra voltage/current sensors are not needed. In addition, this algorithm is realized in the stationary frame, and thus, Park transformations are also not needed. Therefore, the decoupling behavior will not be deteriorated by the PLL dynamics. Moreover, the proposed compensation algorithm is based on the well-known direct modulation and thus can keep stable without extra arm voltage control loops [29], [30]. In addition, the reference compensation signal is very small compared with the original modulation signal. It has an ignorable influence on the voltage balancing between the arms and also cannot break the original stability of the direct modulation.

C. Effect of the Proposed Compensation Algorithm on the Modulation Index

After employing the proposed compensation algorithm, the power control of an MMC can become as simple as that of the conventional two-level VSCs because the power transmission characteristics of them are, now, exactly the same.

Since the proposed algorithm is superposed on the initial modulation reference of the MMC, its effects on the modulation index should be evaluated carefully. In order to do the analysis, both the initial modulation reference and the compensated one should be calculated out. After employing the compensation algorithm, the EMF of the MMC equals exactly the initial modulation reference. Therefore, the initial modulation reference can be calculated based on the power transmission principle as

$$E = \frac{2PX_{\mathrm{eq}}}{3U\sin(\delta)} \tag{17}$$

$$\delta = \arctan\left(\frac{PX_{\mathrm{eq}}}{3U^2/2 - QX_{\mathrm{eq}}}\right) \tag{18}$$

where E is the amplitude of the initial modulation reference and δ is the phase angle difference between the EMF and the grid

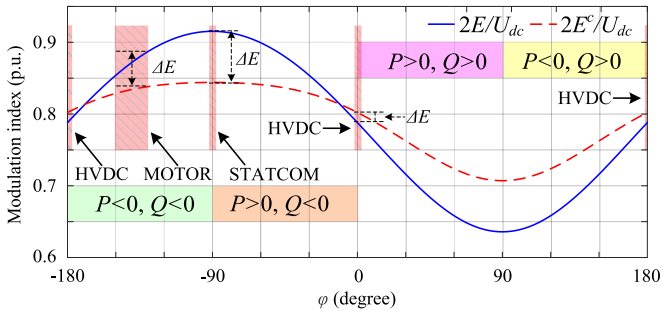

Fig. 9. Modulation indexes of the MMC before and after the compensation.

voltage. P and Q are the transmitted active and reactive powers from the grid to the MMC, respectively. U is the amplitude of the grid phase voltage. $X_{\rm eq} = \omega L_{\rm eq}$ is the ac-side equivalent inductance.

According to (16), the compensation factor is not only related to the initial modulation reference, but also to the sum and difference of the total upper and lower arm capacitor voltage. To simplify the analysis, the circulating current is assumed to be completely eliminated, and the circulating current control factor $U_{\rm cir}$ is much smaller than E. In addition, the losses of the MMC are ignored. Then, based on (4)–(7), the capacitor voltage ripple components can be derived as

$$u_{{\rm cap}j\_1\omega} = \frac{{\rm E}I_{\rm dc}}{U_{\rm dc}\omega C}\cos(\omega t + \delta_{\rm j}) - \frac{I}{4\omega C}\cos(\omega t - \varphi_j) \quad (19)$$

$$u_{{\rm cap}j\_2\omega} = \frac{EI}{8U_{\rm dc}\omega C}\sin(2\omega t + \delta_j - \varphi_j) \quad (20)$$

where $\delta_a = \delta$, $\delta_b = \delta - 2\pi/3$, $\delta_c = \delta + 2\pi/3$, and

$$I = -2P/[3U\cos(\gamma)] \quad (21)$$

$$\gamma = \arctan(Q/P) \quad (22)$$

$$I_{\rm dc} = -P/U_{\rm dc} \quad (23)$$

where γ is the phase angle difference between the grid voltage and current. In the MMC, the odd-order voltage ripple components of the upper and lower arms are opposite, and the even-order ones are the same [18], [19]. So, the sum of the total capacitor voltage of the upper and lower arms can be derived as

$$u_{nj}^{\Sigma} + u_{pj}^{\Sigma} = 2(U_{\rm dc} + nu_{{\rm cap}j\_2\omega}) = 2U_{\rm dc} + \frac{nEI}{4U_{\rm dc}\omega C}\sin(2\omega t + \delta_j - \gamma_j). \quad (24)$$

The difference of the total capacitor voltage of the upper and lower arms can be derived as

$$u_{nj}^{\Sigma} - u_{pj}^{\Sigma} = -2nu_{{\rm cap}j\_1\omega} = -\frac{2n{\rm E}I_{\rm dc}}{U_{\rm dc}\omega C}\cos(\omega t + \delta_j) + \frac{nI}{2\omega C}\cos(\omega t - \gamma_j). \quad (25)$$

Inserting (19), (20), (24), and (25) into (16) and considering that the second SM capacitor voltage ripple is much smaller than the dc voltage, the compensated modulation reference can be derived as

$$e_{j\_{\rm ref}}^{\rm c} = e_{j\_{\rm ref}} + \Delta e_{j\_{\rm ref}} \approx e_{j\_{\rm ref}} + \frac{n{\rm E}I_{\rm dc}}{2U_{\rm dc}\omega C}\cos(\omega t + \delta_j) - \frac{nI}{8\omega C}\cos(\omega t - \gamma_j). \quad (26)$$

The amplitude of the compensated modulation reference can be derived as

$$E^c = \left\{E^2 + \left(\frac{nEI_{\rm dc}}{2U_{\rm dc}\omega C}\right)^2 + \left(\frac{nI}{8\omega C}\right)^2 - \frac{nI}{4\omega C}\left[E^2 + \left(\frac{nEI_{\rm dc}}{2U_{\rm dc}\omega C}\right)^2\right]^{0.5}\sin\left[\delta + \gamma + \arctan\left(\frac{nI_{\rm dc}}{2U_{\rm dc}\omega C}\right)\right]\right\}^{0.5}. \quad (27)$$

According to (17) and (27), the modulation indexes before and after the compensation can be depicted in Fig. 9 with different power factor angle φ (without special statement, all the calculations are based on the circuit parameters listed in Table I). From Fig. 9, when $Q > 0$ (in general), which means the reactive power flows from the grid or load to the MMC, the compensation algorithm can increase the initial modulation index, while when $Q < 0$ (in general), which means the reactive power flows from the MMC to the grid or load, the compensation algorithm can decrease the initial modulation index. It is well known that MMCs are generally used in HVdc transmission, motor drive, and STATCOM. For these applications, their rated operation ranges are all shown in this figure. For example, the power factor of HVdc transmission is usually 1.0 p.u., the motor is about 0.7–0.9 p.u., while STATCOM is –1.0 p.u. As shown in Fig. 9, for HVdc application, the increased modulation index by the compensation algorithm is very small, less than 2%. However, for motor drive and STATCOM applications, the decreased modulation index is much more, about 8% and 4%, respectively, which is very beneficial for practical projects.

TABLE I
MMC PARAMETERS USED IN SIMULATION

Parameters	Value
AC system voltage U_s	220 kV
Rated power S	1000 MVA
AC system inductance L_s	10 mH
Connecting inductance L_c	22 mH
DC-bus voltage U_{dc}	±400 kV
Number of SMs per arm n	400
SM capacitor C	12 mF
SM capacitor voltage U_{cap}	2 kV
Transformer ratio	220 kV/380 kV
Transformer leakage inductance L_T	23 mH
Arm inductance L	55mH

D. Comparison of the Existing and the Proposed Power Decoupling Control Methods for MMCs

In contrast to the existing power decoupling control methods for MMCs, the proposed method offers some different features. A detailed comparison between them is shown in Table II. As shown in this table, six main aspects are listed to make a comparison, and they are explained in detail as follows.

TABLE II
COMPARISON BETWEEN THE EXISTING AND THE PROPOSED POWER DECOUPLING CONTROL METHODS

Decoupling method	Classical method	Improved method [10]	Fully decoupled method [11]	Proposed method
Based on	Simplified control model	Accurate control model	Accurate control model	Compensation algorithm
Structural complexity	Low	Middle	High	Low
Calculation burden	Low	Middle	High	Low
Control accurate	Low	Middle	High	High
Decoupling capability	Part	Part	Full	Full
Control parameters	Two	Three	Two	Two

As to the classical power decoupling method, it has the simplest structure and the lowest calculation burden. However, its decoupling capability is the worst and thus cannot realize accurate power control. It will be seen in the following simulation and experimental results; this decoupling method can result in obvious voltage and current overshoots and unsatisfactory dynamic performance.

As to the improved method, its decoupling capability is much better than the classical one. However, it still cannot realize full power decoupling for the marginally stable property. In addition, it needs to design damping index ζ to achieve an acceptable system damping and decoupling performance. Its structure is more complex, and the calculation burden is also heavier than the classical one. The additional decoupling factors (red terms in Fig. 4) are highly related to the angular frequency provided by the PLL. Therefore, its decoupling dynamic is inevitably affected by the PLL as well.

As to the existing full power decoupling control method, it can completely realize the power decoupling control for MMCs and thus has very high control accuracy. However, its structure is the most complex, and the calculation burden is the heaviest because of cutting off three coupling paths and compensating two influence factors with multiple Park transformations. In addition, the PLL is also closely involved in the decoupling control, which means that the decoupling dynamic is also inevitably affected by the PLL.

As analyzed above, the existing power decoupling methods are all based on the ac current control model. The more accurate the control model, the higher decoupling capability the control method can possess. However, the structure complexity and the calculation burden also increase with the decoupling capability. The proposed power decoupling control method also can realize full power decoupling and has very high control accuracy, just as the existing full power decoupling method. However, different from the existing methods, the proposed method is not based on the accurate control model but a compensation algorithm, and thus, complex/tedious derivation of the ac current control model is not needed. Meanwhile, its structure is very simple, and the calculation burden is also very low. Since this algorithm is realized in the stationary frame, additional Park transformations are not needed, and the PLL is also not involved.

IV. SIMULATION RESULTS

A simulation model of the MMC is established in MATLAB/Simulink to verify the proposed modulation reference compensation method. Fig. 10 presents the structures of the simulation model and the whole control system. The simulation parameters are listed in Table I.

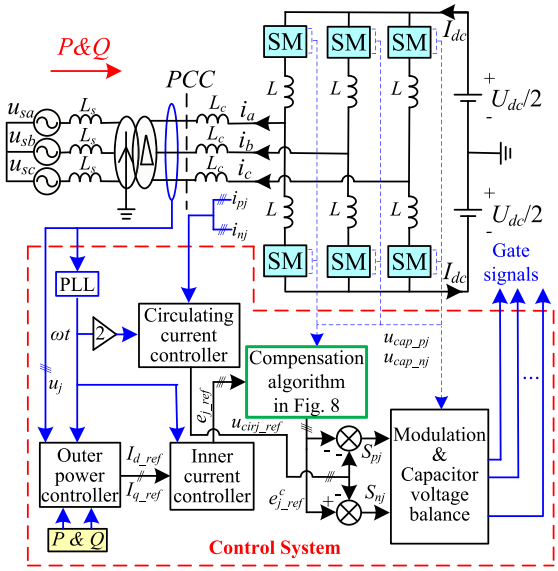

Fig. 10. Structures of the simulation model and the control system.

A. Time-Domain Simulation Results of the Modulation Reference and the EMF of the MMC

To verify the effectiveness and accuracy of the analysis and derivation in Sections III-A, III-B, and III-D, the given modulation references and the output EMFs of MMCs with the classical and the proposed methods are all obtained to make a comparison.

From Fig. 11, it can be seen clearly that there are always some differences between the EMF and the given modulation reference, which conforms to the analysis in Section III-A. These differences are introduced by the internal electrical quantities and control strategies [refer to (11)], and they are exactly the reason resulting in complex power coupling inside the MMC.

From Fig. 12, after adopting the proposed compensation algorithm, the EMF of the MMC is forced to be the same as the given modulation reference, which makes the MMC present the same power transmission characteristics as the conventional VSCs.

From Fig. 13, the compensation algorithm can indeed affect the modulation index of the MMC. Under four typical operation

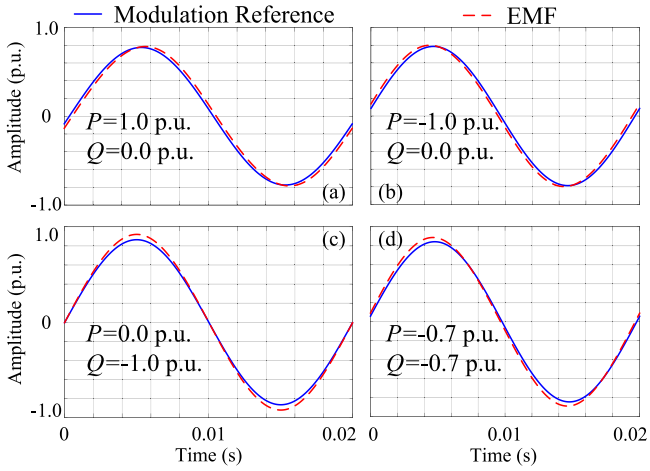

Fig. 11. Modulation reference and EMF of MMCs with the classical power control method.

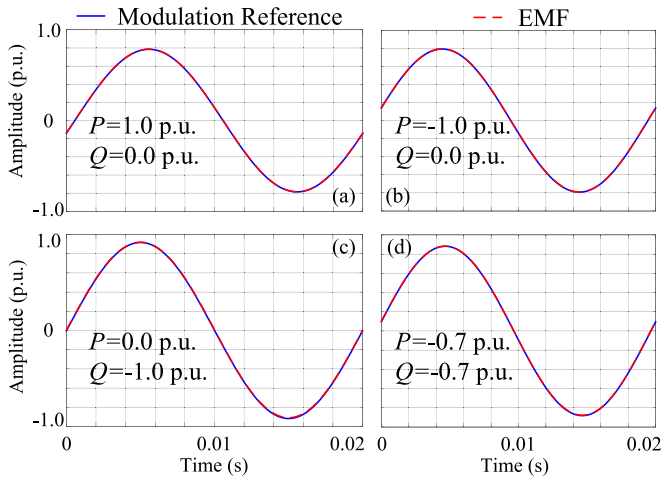

Fig. 12. Modulation reference and EMF of MMCs with the proposed compensation algorithm.

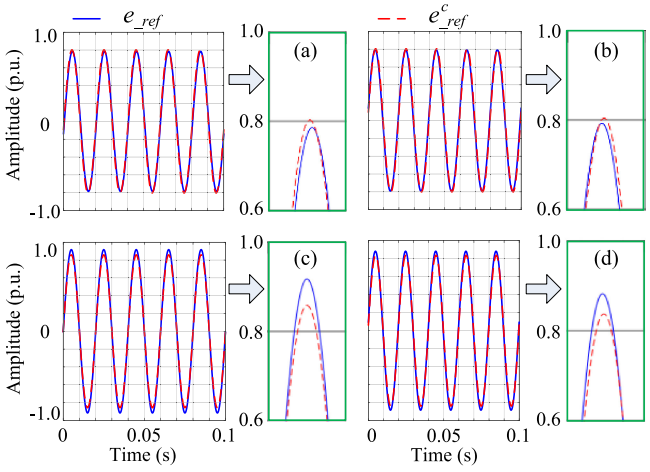

Fig. 13. Initial and compensated modulation references of the MMC with the proposed compensation algorithm under four typical operation conditions.

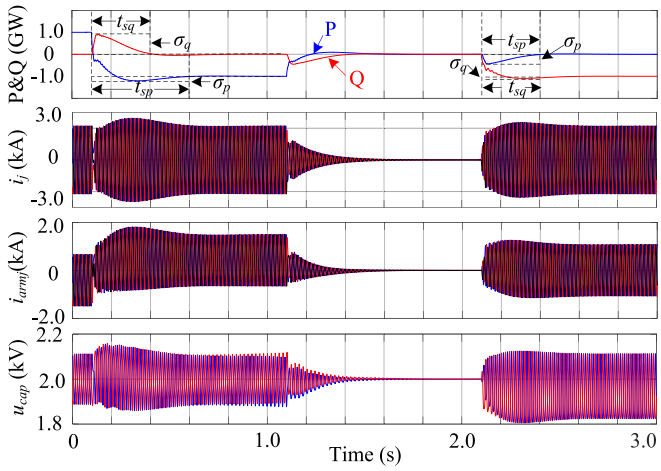

Fig. 14. Simulation results of the classical power decoupling method.

conditions, the simulation results can always fit very well with the calculated results in Section III-D (refer to (17) and (27) as well as Fig. 9).

B. Comparison of Simulation Results With Different Power Decoupling Methods

Before 0.1 s, the MMC operates at rated power ($P = 1.0$ p.u. and $Q = 0$) in a steady state and then P reverses ($P = -1.0$ p.u. and $Q = 0$), and 1.0 s later, P changes to 0 ($P = 0$ and $Q = 0$). At 2.1 s, Q steps from 0 to -1.0 p.u. ($P = 0$ and $Q = -1.0$ p.u.). In this paper, the ac current controller is designed as a first-order control structure, which is a widely used design method in VSCs. The time constant of the ac current controller is the same for both the classical and the proposed control methods. The coupling inside the classical control structure/controller cannot be eliminated with control parameter tuning but only decoupling structures [9], [10].

The classical power decoupling method, the existing full power decoupling method, and the proposed compensation method are all simulated to make a comparison. Fig. 14 presents the active power P, reactive power Q, ac current i_j, arm current $i_{\mathrm{arm}j}$, and SM capacitor voltages u_{cap} of the upper and lower arms after employing the classical power decoupling method. Figs. 15 and 16 show the corresponding electrical quantity simulation results of the existing full power decoupling method and the proposed compensation method, respectively.

From these figures, the electrical quantities of the MMC present different dynamic performances with different power decoupling strategies. To describe the dynamic performance conveniently, two indexes, the power overshoot (σ) and the power step settling time (t_s), are defined. σ refers to the first peak value subtracts the steady-state value during power step response. t_s is the moment when the error to the steady-state value is less than 2%. From these figures, obvious active and reactive power overshoots (σ_p and σ_q) and a much longer step settling time (t_{sp} and t_{sq}) can be observed in Fig. 14, which means power decoupling cannot be completely achieved with the classical method. In addition, the ac currents, arm currents,

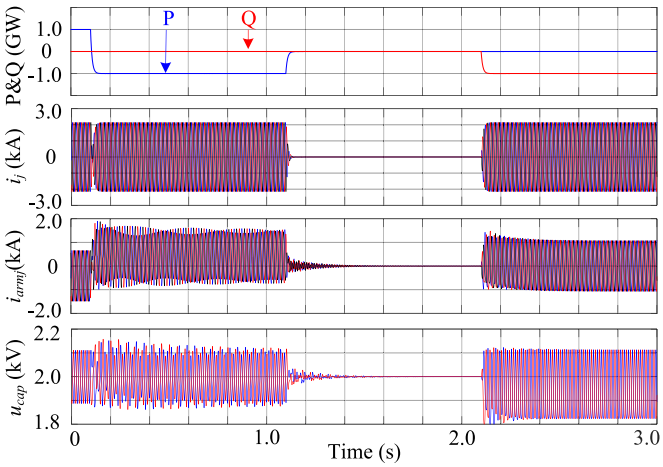

Fig. 15. Simulation results of the full power decoupling method.

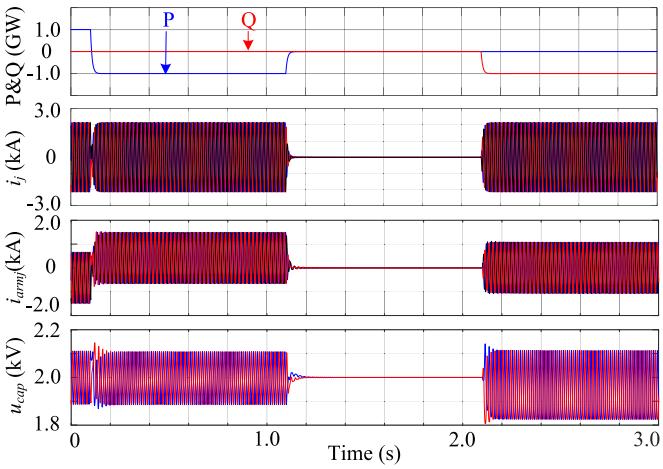

Fig. 16. Simulation results of the proposed compensation method.

and SM capacitor voltages present much longer step settling time and also obvious overshoots when employing the classical method. Although the settling time of the classical method can be further reduced with a smaller control time constant, especially in some low-time-delay or high-sampling-frequency MMC systems [31], the simulation here is just for a generally purpose and mainly used to present the obvious coupling effects between the active and reactive powers.

However, from Figs. 15 and 16, the power step performance likes that of an ideal first-order control system. There are no power overshoots and coupling effects between the active and reactive powers, which means both the existing full power decoupling method and the proposed compensation method can completely realize the active and reactive power decupling control for the MMC. Meanwhile, the ac current for these two power decoupling methods is also very ideal, just as the dynamic performance of a quasi-ideal first-order control system, which is very similar to the theoretical value.

As to the arm currents and SM capacitor voltages, there appear obvious high-frequency ripples with the existing full power decoupling method. For example, the settling time of the arm current is about 600 ms because of the high-frequency ripple, and the maximum ripple amplitude is about 320 A. The settling time of the SM capacitor voltage is about 650 ms, and the maximum ripple amplitude (peak to peak) is about 300 V. These may be caused by the PLL dynamic and/or the method itself. Since this paper concentrates on proposing a new power decoupling control method, the detailed analysis and validation of the existing methods will be the future work. The settling time of the arm current and capacitor voltage in Fig. 16 is very small (about 30 and 40 ms, respectively), and the corresponding ripples are also very small, e.g., there is no arm current ripple, and the ripple amplitude (peak to peak) of the capacitor voltage is about 260 V.

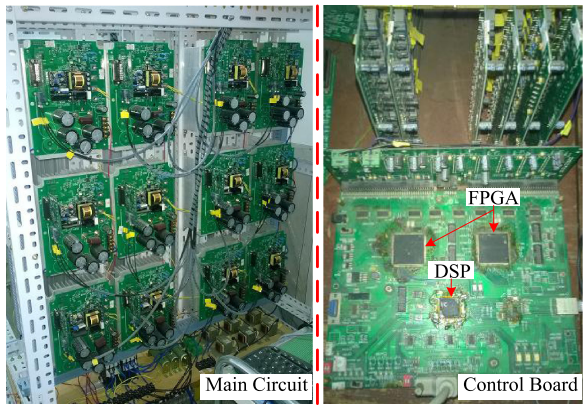

Fig. 17. Experimental setup.

All in all, the classical power decoupling method cannot fully realize power decoupling, and thus, there appears apparent power, ac current, arm current, and capacitor voltage overshoots, which may result in overload operation and increases the electrical stresses of circuit components. Moreover, this can result in malfunctions of the protection circuits and thus threatens the normal operation of the MMC. In addition, the electrical quantity dynamic response is relatively slow.

The proposed compensation method, which is much simpler than the existing full power decoupling method, can realize fully decoupled power control for the MMC, and thus, the powers and ac currents can present "ideal" dynamic performance. In addition, other electrical quantities, such as the arm currents and SM capacitor voltages, also present more appropriate dynamic performance compared with the existing decoupling methods.

V. Experimental Validations

A 10-kVA/±400-V downscaled MMC prototype is built to verify the proposed modulation reference compensation method. Fig. 17 shows the experimental prototype and the control platform. Table III lists the detailed parameters of the prototype.

In the experiment, a phase-shifted pulsewidth modulation method [20] and a sorting method [25] are employed. The switching frequency of IGBTs is set to 625 Hz. In the experiments, both the classical and the proposed methods are carried out to make a comparison.

TABLE III
PARAMETERS OF THE MMC PROTOTYPE

Parameters	Value
AC system voltage U_s	380 V
Rated power S	10 kVA
AC-side inductance L_c	2.5 mH
DC-bus voltage U_{dc}	±400 V
Number of SMs per arm n	4
SM capacitor C	1200 μF
SM capacitor voltage U_{cap}	200 V
Arm inductance L_a	5 mH

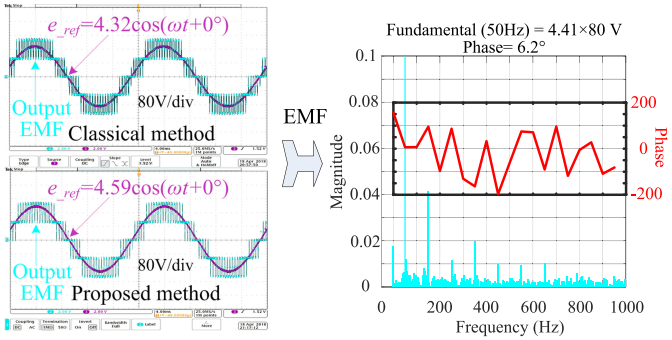

Fig. 18. Experimental results of the modulation references and EMFs of the MMC, when $P = -7$ kW and $Q = -7$ kVar.

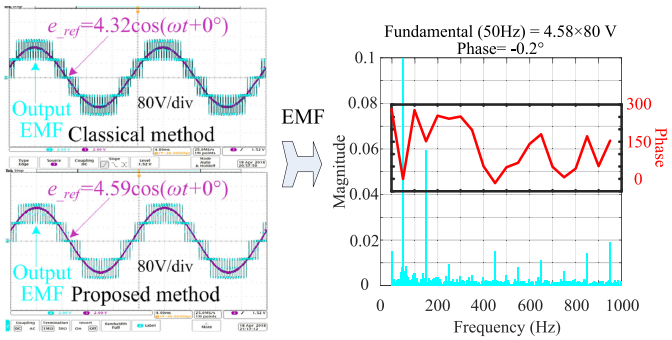

Fig. 19. Experimental results of the modulation references and EMFs of the MMC, when $P = 0$ and $Q = -10$ kVar.

Figs. 18 and 19 present the experimental results of the given modulation references and the output EMFs of the MMC under two different operation conditions. In general, it is difficult to accurately and clearly compare the output EMFs and the given modulation references because the output EMFs contain the switching harmonics and sideband harmonics for the switching actions of the IGBTs. Therefore, the fundamental frequency components of the output EMFs need to be extracted by fast Fourier transformation (FFT) to make comparison. The right subfigures in Figs. 18 and 19 are the FFT results of the output EMFs including both magnitudes and phases.

It can be seen from Figs. 18 and 19 that the modulation references ($e_{\_\mathrm{ref}}$ in the top left subfigure) and the fundamental frequency components of the output EMFs (the FFT results in the right subfigure) are obviously different when employing the classical control method. For example, the magnitudes are, respectively, 4.20 and 4.41 V (all the magnitude values have already been divided by 80 to capture by the oscilloscope) and the phases are, respectively, 4.3° and 6.2° when $P = -7$ kW and $Q = -7$ kVar, and the magnitudes are, respectively, 4.32 and 4.58 V when $P = 0$ and $Q = -10$ kVar. However, when employing the proposed method, the modulation references ($e_{\_\mathrm{ref}}$ in the down left subfigure) and the fundamental frequency components of the output EMFs are almost the same, and the magnitude and phase errors are ignorable.

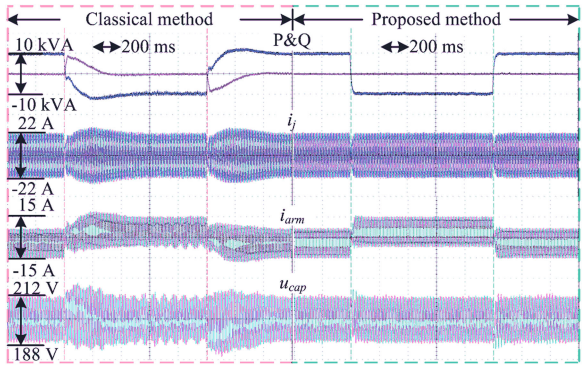

Fig. 20. Experimental results when P changes.

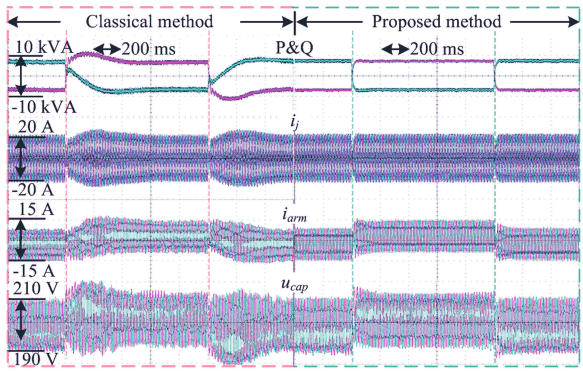

Fig. 21. Experimental results when both P and Q change.

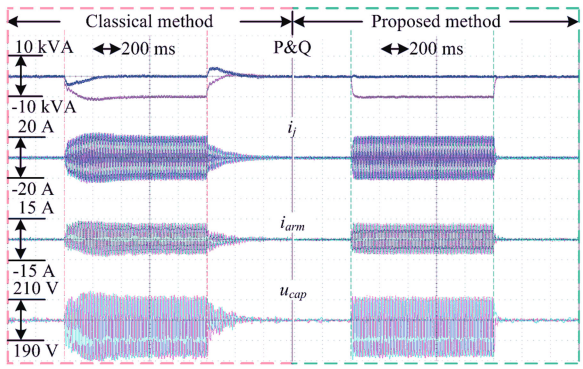

Fig. 22. Experimental results when Q changes.

Figs. 20–22 present, from the top to the bottom, the experimental results of the active and reactive powers, ac current, arm current, and SM capacitor voltages when the active power change (from 10 to −10 kW), both the active and reactive power

change (from 7 to −7 kW; from −7 to 7 kVar), and the reactive power change (from 0 to −10 kVar) occur, respectively.

From Figs. 20–22, active power change always causes obvious reactive power change and vice versa after adopting the classical control method. In addition, the dynamic performance of electrical quantities does not confirm to the theoretical analysis, e.g., the settling time is much longer, and there also appearing evident overshoots. However, after employing the proposed compensation method, the coupling effect between the active and reactive powers is completely eliminated. Therefore, there does not appear any obvious electrical quantity overshoots, and their settling time is very close to the theoretical values, which greatly improves the dynamic performance and operation safety of the MMC system. The whole MMC system dynamic performance conforms to an ideal first-order control system, which further verifies the effectiveness and accuracy of the proposed compensation method and the corresponding theoretical analysis in Section IV-B.

VI. Conclusion

This paper proposes a method to realize fully decoupled power control for MMCs. Different from the existing methods, it is not based on the control model, but forces the output EMF of MMCs to be the same as the given modulation reference by a real-time compensating/amending algorithm. Therefore, the power transmission characteristics of MMCs are changed to be exactly the same as the conventional VSCs. Since the proposed method is essentially a compensation algorithm in the stationary frame, it is very easy to implement in a microcontroller with low calculation burden, and its decoupling dynamics are not involved with the PLL. In addition, the proposed method does not need tedious accurate control model derivation and additional control parameter design or voltage/current sensors, which is very beneficial to practical projects. The realization process and the effects of the compensation algorithm on the modulation index are introduced and analyzed in detail. The proposed modulation reference compensation method finally realizes accurate and fully decoupled power regulation for the MMC and thus avoids the overload operation and protection malfunction and significantly improves the system dynamic performance. The effectiveness and accuracy of the proposed analysis and compensation method are carefully verified by both simulation and experimental results under different operation conditions.

References

[1] S. Debnath and M. Saeedifard, "A new hybrid modular multilevel converter for grid connection of large wind turbines," *IEEE Trans. Sustain. Energy*, vol. 4, no. 4, pp. 1051–1064, Oct. 2013.

[2] A. Nami, J. Liang, F. Dijkhuizen, and G. D. Demetriades, "Modular multilevel converters for HVDC applications: Review on converter cells and functionalities," *IEEE Trans. Power Electron.*, vol. 30, no. 1, pp. 18–36, Jan. 2011.

[3] M. Hagiwara, K. Nishimura, and H. Akagi, "A medium-voltage motor drive with a modular multilevel PWM inverter," *IEEE Trans. Power Electron.*, vol. 25, no. 7, pp. 1786–1799, Jul. 2010.

[4] H. Mohammadi and M. Bina, "A transformerless medium-voltage STATCOM topology based on extended modular multilevel converters," *IEEE Trans. Power Electron.*, vol. 26, no. 5, pp. 1534–1545, May 2011.

[5] T. Soong and P. W. Lehn, "Assessment of fault tolerance in modular multilevel converters with integrated energy storage," *IEEE Trans. Power Electron.*, vol. 31, no. 6, pp. 4085–4095, Jun. 2016.

[6] Z. Liu *et al.* , "The start control strategy design of unified power quality conditioner based on modular multilevel converter," in *Proc. IEEE Int. Electr. Mach. Drives Conf.*, May 2013, pp. 933–937.

[7] K. Dai, P. Liu, Y. Kang, and J. Chen, "Decoupling current control for voltage source converter in synchronous rotating frame," in *Proc. 4th IEEE Int. Conf. Power Electron. Drive Syst.*, Oct. 2001, vol. 1, pp. 39–43.

[8] B. Bahrani, S. Kenzelmann, and A. Rufer, "Multivariable-PI-based *dq* current control of voltage source converters with superior axis decoupling capability," *IEEE Trans. Ind. Electron.*, vol. 58, no. 7, pp. 3016–3026, Jul. 2011.

[9] H. Yang, W. Li, L. Lin, and X. He, "Decoupled current control with synchronous frequency damping for MMC considering sub-module capacitor voltage ripple," *IEEE Trans. Power Del.*, vol. 33, no. 1, pp. 419–428, Feb. 2018.

[10] J. Wang and P. Wang, "Power decoupling control for modular multilevel converters," *IEEE Trans. Power Electron.*, vol. 33, no. 11, pp. 9296–9309, Nov. 2018.

[11] D. H. Pham, G. Hunter, L. Li, and J. Zhu, "Feedforward decoupling control method in grid-interfaced inverter," in *Proc. Australas. Univ. Power Eng. Conf.*, pp. 1–5, 2013.

[12] B. Bahrani, A. Karimi, B. Rey, and A. Rufer, "Decoupled *dq*-current control of grid-tied voltage source converters using nonparametric models," *IEEE Trans. Ind. Electron.*, vol. 60, no. 4, pp. 1356–1366, Apr. 2013.

[13] Y. Wang, W. Wang, C. Wang, and X. Wu, "Coupling analysis on current control at low switching frequency for the three-phase PWM converter based on RGA and a novel output feedback decoupling method," *IEEE Trans. Ind. Electron.*, vol. 63, no. 11, pp. 6684–6694, Nov. 2016.

[14] E. Solas, G. Abad, J. Barrena, S. Aurtenetxea, A. Carcar, and L. Zajac, "Modular multilevel converter with different submodule concepts—Part I: Capacitor voltage balancing method," *IEEE Trans. Ind. Electron.*, vol. 60, no. 10, pp. 4525–4535, Oct. 2013.

[15] E. Solas, G. Abad, J. Barrena, S. Aurtenetxea, A. Carcar, and L. Zajac, "Modular multilevel converter with different submodule concepts—Part II: Experimental validation and comparison for HVDC application," *IEEE Trans. Ind. Electron.*, vol. 60, no. 10, pp. 4536–4545, Oct. 2013.

[16] D. Ludois and G. Venkataramanan, "Simplified terminal behavioral model for a modular multilevel converter," *IEEE Trans. Power Electron.*, vol. 29, no. 4, pp. 1622–1631, Apr. 2014.

[17] L. Harnefors, A. Antonopoulos, S. Norrga, L. Angquist, and H.-P. Nee, "Dynamic analysis of modular multilevel converters," *IEEE Trans. Ind. Electron.*, vol. 60, no. 7, pp. 2526–2537, Jul. 2013.

[18] Q. Song, W. Liu, X. Li, H. Rao, S. Xu, and L. Li, "A steady-state analysis method for a modular multilevel converter," *IEEE Trans. Power Electron.*, vol. 28, no. 8, pp. 3702–3713, Aug. 2013.

[19] J. Wang, J. Liang, F. Gao, X. Dong, C. Wang, and B. Zhao, "A closed-loop time-domain analysis method for modular multilevel converter," *IEEE Trans. Power Electron.*, vol. 32, no. 10, pp. 7494–7508, Oct. 2017.

[20] Q. Tu, Z. Xu, and L. Xu, "Reduced switching-frequency modulation and circulating current suppression for modular multilevel converters," *IEEE Trans. Power Del.*, vol. 26, no. 3, pp. 2009–2017, Jul. 2011.

[21] S. Fan, K. Zhang, J. Xiong, and Y. Xue, "An improved control system for modular multilevel converters with new modulation strategy and voltage balancing control," *IEEE Trans. Power Electron.*, vol. 30, no. 1, pp. 358–371, Jan. 2015.

[22] Z. Li, P. Wang, Z. Chu, H. Zhu, Y. Luo, and Y. Li, "An inner current suppressing method for modular multilevel converters," *IEEE Trans. Power Electron.*, vol. 28, no. 11, pp. 4873–4879, Nov. 2013.

[23] X. Li, Q. Song, W. Liu, S. Xu, Z. Zhu, and X. Li, "Performance analysis and optimization of circulating current control for modular multilevel converter," *IEEE Trans. Ind. Electron.*, vol. 63, no. 2, pp. 716–727, Feb. 2016.

[24] L. He, K. Zhang, J. Xiong, and S. Fan, "A Repetitive control scheme for harmonic suppression of circulating current in modular multilevel converters," *IEEE Trans. Power Electron.*, vol. 30, no. 1, pp. 471–481, Jan. 2015.

[25] D. Siemaszko, "Fast sorting method for balancing capacitor voltages in modular multilevel converters," *IEEE Trans. Power Electron.*, vol. 30, no. 1, pp. 463–470, Jan. 2015.

[26] P. M. Meshram and V. B. Borghate, "A simplified nearest level control (NLC) voltage balancing method for modular multilevel converter (MMC)," *IEEE Trans. Power Electron.*, vol. 30, no. 1, pp. 450–462, Jan. 2015.

[27] X. Shi, Z. Wang, B. Liu, Y. Liu, L. M. Tolbert, and F. Wang, "Characteristic investigation and control of a modular multilevel converter-based HVDC system under single-line-to-ground fault conditions," *IEEE Trans. Power Electron.*, vol. 30, no. 1, pp. 408–421, Jan. 2015.
[28] Q. Tu, Z. Xu, Y. Chang, and L. Guan, "Suppressing DC voltage ripples of MMC–HVDC under unbalanced grid conditions," *IEEE Trans. Power Del.*, vol. 27, no. 3, pp. 1332–1338, Jul. 2012.
[29] Y. Sun, C. Teixeira, D. Holmes, B. McGrath, and J. Zhao, "Low-order circulating current suppression of PWM-based modular multilevel converters using dc-link voltage compensation," *IEEE Trans. Power Electron.*, vol. 33, no. 1, pp. 210–225, Jan. 2018.
[30] M. Sleiman, K. Al-Haddad, H. F. Blanchette, and H. Y. Kanaan, "Insertion index generation method using available leg-average voltage to control modular multilevel converters," *IEEE Trans. Ind. Electron.*, vol. 65, no. 8, pp. 6206–6216, Aug. 2018.
[31] K. Sharifabadi, L. Harnefors, H. P. Nee, S. Norrga, and R. Teodorescu. *Design, Control, and Application of Modular Multilevel Converters for HVDC Transmission Systems*. New York, NY, USA: Wiley, 2016.

Jinyu Wang (S'15–M'17) received the B.Eng. degree in electrical engineering and the M.Eng. degree in power electronics from Jilin University, Changchun, China, in 2010 and 2013, respectively, and the Ph.D. degree in power system from Shandong University, Jinan, China, in 2017.

He is currently a Research Fellow with Nanyang Technological University, Singapore. His current research interests include modeling and control of grid-integrated power converters, in particular, stability analysis and control of modular-multilevel-converter-based HVdc.

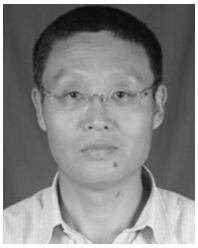

Peng Wang (M'00–SM'11–F'17) received the B.Sc. degree from the Xi'an Jiaotong University, Xi'an, China, in 1978, the M.Sc. degree from the Taiyuan University of Technology, Taiyuan, China, in 1987, and the M.Sc. and Ph.D. degrees from the University of Saskatchewan, Saskatoon, SK, Canada, in 1995 and 1998, respectively.

He is currently a Professor with Nanyang Technological University, Singapore.

Michael Zagrodnik received the B.A.Sc. degree in engineering science from the University of Toronto, Toronto, ON, Canada, in 1989, and the M.Sc. degree in electrical engineering from the National University of Singapore, Singapore, in 1995.

He was with Vestas Wind Systems. He is currently with Rolls-Royce Singapore Pte. Ltd., Singapore, where he works primarily in the area of high-power converters for marine and aircraft propulsion. His research interests include renewable energy integration, drives, and power electronic converters.

Suvajit Mukherjee (SM'15) received the B.E. degree in electrical engineering from the Indian Institute of Engineering Science and Technology, Shibpur, India, in 2001, the M.E. degree in electrical engineering from Jadavpur University, Kolkata, India, in 2004, and the Ph.D. degree in electrical engineering from the Indian Institute of Technology, Kharagpur, India, in 2008.

Since 2007, he has worked in various power industries like Emerson Network Power, Optimal Power Solutions, and Stesalit Limited. He is currently with Rolls-Royce Singapore Pte. Ltd., Singapore. His research interests include multilevel converters, high-voltage converters, control of high-power drives, sensorless ac motor control, uninterruptible power systems, solar inverters, and battery charging.

Dhanashree Vaidya received the B.Tech. degree in electronics and telecommunication from the College of Engineering, Pune, India, in 2013, and the M.Sc. degree in embedded systems from Nanyang Technological University, Singapore, in 2015.

She is currently a Research Associate with Rolls-Royce @NTU Corporate Lab, Nanyang Technological University. Her current research focuses on developing control and communication systems for power converters used in marine and aerospace.